scientific reports

Check for updates

OPEN

Investigation of polypyrrole based composite material for lithium sulfur batteries

Veronika Niščáková[1], Alexandra Gubóová[1], Ondrej Petruš[2], Haojie Fei[3], Miroslav Almáši[4] & Andrea Straková Fedorková[1]✉

With the rising demand for electricity storage devices, the performance requirements for such equipment have become increasingly stringent. Lithium-sulfur (Li-S) batteries are poised to be among the next generation of energy storage systems. However, before they can be commercially viable, several challenges must be addressed, including low sulfur conductivity and the shuttle effect. Herein, polypyrrole based sulfur composite was prepared by simple method in hydrothermal teflon lined autoclave for Li-S battery. The S/SP/ppy/PVDF electrode exhibited the initial discharge capacity of 662 mAh g^{-1} at 0.5 C and 637 mAh g^{-1} after 100 cycles. The Coulombic efficiency was 96% all along charge/discharge cycling. Moreover, Li-S coin cells were assembled and tested to demonstrate the potential application and scale-up of the polypyrrole-sulfur composite.

Keywords Polypyrrole, Cathode materials, Energy storage, Lithium-sulfur batteries

Energy crisis and rapid depletion of fossil fuels are pressing issues that prompt research and development of alternative, sustainable, and preferably renewable energy sources[1]. Widely used Li-ion batteries (LIBs) are not able to supply such a demand anymore. By using sulfur instead as an active material, lithium-sulfur batteries (Li-S) not only immensely increase their theoretical energy density (2600 Wh.kg^{-1} as opposed to roughly 460 Wh.kg^{-1} of LIBs), but they also relieve the environment by not using additional critical raw materials[2]. Sulfur is an earth abundant element with high theoretical specific capacity of 1675 mAh.g^{-1}[3]. Despite issues hindering their full industrial applications, such as shuttle effect or capacity fade, Li-S batteries have potential to achieve practical energy density of 500–600 Wh.kg^{-1}[4]. For this reason, a lot of research is focused on modifications and improvements that would help overcome mentioned disadvantages[5–8]. One of the approaches is minimizing shuttle effect, which is a phenomenon that occurs when lithium polysulfide intermediates dissolve during charge/discharge process, and can be suppressed by anchoring of sulfur cathode via chemical adsorption or physical confinement[9]. Sulfur, despite its high theoretical capacity, exhibits poor electrical conductivity. This inherent limitation must be addressed to enable the commercialization of lithium-sulfur batteries. One potential solution involves encapsulating sulfur within a conductive material. This approach would facilitate enhanced lithium ion transfer and simultaneously sequester the polysulfides generated during the battery's operation within the conductive matrix, thereby addressing both the conductivity and polysulfide shuttle issues concurrently[10].

Conjugated polymers with great conductivity even similar to metals, known as conducting polymers are widely utilized in energy storage or power generation technologies due to their unique metallic/semiconductor properties, and high redox potential[11]. Structural conducting polymers are polymers that are able to reach conductive properties by their own structures, such as polypyrrole (ppy), polyaniline or polythiophene[2].

Polypyrrole is a nontoxic heterocyclic structure that contains nitrogen. It can be prepared in many different forms such as powder (nanoparticles, nanotubes…), sponge or thin film coatings[12]. It shows a lot of promise thanks to its great conductivity, cost effectiveness, and facile synthesis[13]. It can be commonly synthetized either by electrochemical polymerization or low temperature oxidation polymerization. Polypyrrole can be used in many types of batteries such as LiBs, Li-S, Aqueous zinc-ion batterie or Sodium based dual-ion batteries. By employing different ppy composite cathodes with properly tuned properties, high performances can be achieved. Addition of ppy into cathode can improve not only electrochemical performance, but it can also enhance stability, increase cyclability, discharge capacity, and provide better electron transport[14].

[1]Department of Physical Chemistry, Faculty of Sciences, Pavol Jozef Šafárik University in Košice, Moyzesova 11, Košice 04154, Slovak Republic. [2]Institute of Materials Research, Slovak Academy of Sciences, Watsonova 47, Košice 040 01, Slovak Republic. [3]Centre of Polymer Systems, Tomas Bata University in Zlín, Zlín 760 01, Czech Republic. [4]Department of Inorganic Chemistry, Faculty of Sciences, Pavol Jozef Šafárik University in Košice, Moyzesova 11, Kosice 04154, Slovak Republic. ✉email: andrea.fedorkova@upjs.sk

Sun et al.[15] examined ppy as stable and ultrafast cathode material in dual-ion batteries due to its reversible doping mechanism. Prepared sodium based dual-ion batteries showed remarkable lifespan 3000 cycles with 83% capacity retention. And reversible capacity of 125 $mAh.g^{-1}$. Excellent performance was linked to fast redox kinetics[15]. Pathak et al.[16] synthetized a polypyrrole coated nanocomposite sulfur cathode with addition of Li_2S_6 electrolyte. S-ppy electrode showed a low capacity decay of only 0.31% per cycle with 165 cycles at 0.2 Ag^{-1}. The post mortem studies revealed that Li_2SO_4 protective layer was formed on the electrodes and ppy coating which resulted in entrapment of lithium polysulfides in the cathode[16]. Luna-Lama et al.[17] investigated effects of dual copolymers, specifically polypyrrole and polystyrene sulfonate and found out this combination enhances the conductivity of electrode. At 0.1 C after 250 cycles the copolymer reached 1200 $mAh.g^{-1}$ and at 5 C after 500 cycles it was 640 $mAh.g^{-1}$ meaning it performs well at low and high current densities. Moreover, it helps to decrease the polysulfide migration, which was explained by heteroatoms (N, O, S) present in the structure[17]. Li et al.[18] designed ppy-coated sulfur/graphene aerogel composite material with very slow decay rate of 0.03% per cycle after 500 cycles at 0.5 C. The graphene acts as a 3D network and encapsulated sulfur particles. The ppy layer assumes the role of a host and a chemical adsorbent to effectively minimize dissolution of lithium polysulfides and ensure stable cycling[18]. Wei et al.[19] studied porous polypyrrole modified SnO_2 nanotubes for encapsulation of sulfur particles for efficient enhancement of the charge transfer capabilities. Advantageous and cost-effective design with conductive ppy and metal oxide showed promising results with rate performance of 383.7 $mAh.g^{-1}$ at 5 C and remarkable stability after 500 cycles at 1 C with decay 0.05% per cycle[19].

The aim of this work was to prepare polypyrrole based composite material for lithium-sulfur cathode by easy and scalable room temperature polymerization. By adding polypyrrole, the conductivity was increased, and shuttle effect was minimized by entrapment of polysulfide intermediates. The successful synthesis of polymerized pyrrole was characterized using infrared spectroscopy (IR), Raman spectroscopy, and powder X-ray diffraction (PXRD). Subsequently, polymerized pyrrole was employed as a matrix for a sulfur cathode, resulting in the fabrication of a S/SP/ppy/PVDF positive electrode. The morphology of the prepared positive electrode was examined using scanning electron microscopy (SEM), supplemented by an energy dispersive X-Ray analysis (EDX). Electrochemical properties were analyzed through electrochemical impedance spectroscopy (EIS), cyclic voltammetry (CV), and galvanostatic cycling (GC). Prepared material was electrochemically characterized in two-electrode configuration electrochemical testing cell (El-Cell). Additionally, coin cell prototype was prepared and tested to illustrate possibilities of industrial application.

Materials and methods

Chemicals

Sulfur (Sigma-Aldrich), carbon Super P (Alfa Aesar), PVDF (polyvinylidene difluoride) (Sigma-Aldrich), $FeCl_3$ (CentralChem), pyrrole (Sigma-Aldrich), NMP (N-methyl-2-pyrrolidone) (Sigma-Aldrich), metal lithium (Sigma-Aldrich), glass fiber-based separator (Whatman), lithium nitrate ($LiNO_3$) (Acros Organics), lithium bis(trifluoromethanesulfonyl) imide (LiTFSI) (Sigma-Aldrich), 1,2- dimethoxyethane (DME) (Sigma-Aldrich), 1,3-dioxolane (DOL) (Sigma-Aldrich), ethanol (Centralchem).

Material synthesis

Polypyrrole was prepared by oxidative polymerization of pyrrole monomer using $FeCl_3$ as an oxidizing agent. Firstly, a solution of $FeCl_3$ (0.5 M) was prepared. Pyrrole was then added dropwise to this solution, and the mixture was stirred for 2 h on a magnetic stirrer without heating (laboratory temperature). The resulting black polypyrrole was separated by filtration and washed with dilute HCl and with distilled water. Finally, the filtered and washed ppy was dryed in an air oven at a temperature of 60 °C.

Sulphur, carbon super P and polypyrrole (wt% 60:25:15) were transferred to a sealable Teflon Lined Hydrothermal Autoclave and left on air oven for 4 h at a temperature of 140 °C, resulting in the preparation of a S/SP/ppy composite.

Preparation of cathodes and cells assembly

Initially, slurry formulated by combining the S/SP/ppy composite (90 wt%) in the specified quantity of NMP, augmented with PVDF (10 wt%), and allowed to be blended for a duration of 24 h was prepared. Utilizing the doctor blade technique, the prepared slurry was administered onto aluminum foil which serve as the current collector and have supplementary carbon modification to enhance its conductivity. The aluminum foil, coated with the aforementioned slurry, underwent a 24-hour drying process in an air oven set at 60 °C. Following the drying, electrodes with a diameter of 18 mm were excised. Subsequently, these electrodes underwent compression using a hydraulic press at a pressure of approximately 300 $kg.cm^{-2}$ and were subsequently subjected to drying within an argon atmosphere at 60 °C for a duration of 24 h. The test cells (El-Cell) were assembled within the argon-filled glove box provided by Jacomex. The electrodes that had been prepared were subsequently utilized as working electrodes in the test cell (El-cell). Metal lithium functioned as counter and reference electrode. The glass fiber separator underwent impregnation with an electrolyte characterized by a composition of 0.25 M $LiNO_3$ and 0.7 M LiTFSI solution in DME and DOL, with a volume ratio of DME to DOL at 2:1. The coin cell prototypes (CR2032) were assembled with S/Super P/ppy composite as the working electrode, Li metal chip as the counter and reference electrode, and polypropylene film (Celgard 2500) as the separator. The diameter of the working electrode was 14 mm and the amount of electrolyte added was 50 µL.

Material characterization

For morphological characterization, two different scanning electron microscopes— JSM-7000 F (JEOL), and SEM EVO MA15—each equipped with an energy-dispersive X-ray detector. Raman spectra were acquired using an XploRA ONE spectrometer, which is equipped with a 532 nm laser operating at 50 mW power. The acquisition

parameters included an accumulation time of 10 s with double repetition. PXRD analysis was measured by a Philips X'Pert Pro laboratory X-ray tube in a Bragg-Brentano setup with a Cu lamp with wavelengths $_1 = 1.54056$ Å and $_2 = 1.54439$ Å at room temperature.

The infrared spectra of compounds used for the preparation of polypyrole and the cathode material were measured on an AVATAR 6700 (Thermo Scientific) instrument by ATR (attenuated total reflectance, pyrole) or KBr method (polypyrole, sulphur, Super P and cathode composite) in the wavenumber range of 4000 –400 cm^{-1}. Before measurements, KBr was dried at 600 °C to remove water moisture from the compound. The samples were prepared as KBr tablets with a mass ratio of 1/100 (compound/KBr) and measured using the transmission technique. For each KBr and ATR spectra, 32 or 64 repetitions of scans were recorded, with a resolution of 4 cm^{-1}, respectively.

The thermal behaviour and stability of the compounds was studied on the STA 449 F1 Jupiter apparatus (Netzsch). The samples were heated in the temperature range of 30–800 °C with a heating rate of 10 °C min^{-1} in an air atmosphere. The mass of the analyzed compounds was in the range of 10–20 mg. To remove the mass changes corresponding to solvents, thermogravimetric (TG) curves were normalized according to the procedure described in[20].

Electrochemical characterization

Electrochemical impedance spectroscopy, cyclic voltammetry, and galvanostatic cycling measurements using potentiostats (PGSTAT101 and Bio-Logic VSP-3e) were used for electrochemical characterization of prepared cathodes. EIS were done in the frequency range of 1 MHz–100 mHz with an amplitude of 10 mV, before and after long-term cycling. The CV was measured in the potential from 1.8 V to 2.8 V with scan rates of 0.1; 0.5; 1 and 2 mV s^{-1}. GC was accomplished at the voltage range between 1.8 V and 2.8 V vs. Li^+/Li at different C-rates, and long-term cycling (100 cycles) at 0.5 C.

Results and discussion

Surface and structural characterization

SEM was employed to scrutinize the surface morphology of the prepared electrode, concurrently utilizing EDX analysis for ascertaining the composition of the examined sample and elucidating the distribution of individual elements therein. The images were obtained at various magnifications, specifically 500x, 2000x, 5000x, and 10,000x, and are depicted in the Fig. 1a–d. The SEM analysis reveals that the surface morphology of the electrode, following the introduction of ppy to the cathode material, exhibits some non-uniformity, characterized by noticeable fissures. While the electrode's surface shows microporosity, this feature might not be distinctly apparent in the images provided. Additionally, sulfur clusters, observed as spherical particles approximately 1 µm in diameter, are randomly dispersed throughout the electrode. These clusters exhibit a size range of 3 to 20 µm, as depicted in Fig. 1, though some variation in distribution and size may occur across different regions of the electrode.

Energy-dispersive X-ray spectroscopy analysis was conducted to discern the composition of the examined sample. The replying EDX spectrum from analyzed area (Fig. 2a) is depicted in the Fig. 2b. Notably, the manifestation of fluorine, attributed to the binder employed (PVDF), is evident. Additionally, the presence of sulfur and carbon, integral components employed in the synthesis of the cathode material, is identified. A comprehensive summary of atomic and mass percentages is presented in the accompanying Table 1. The Fig. 2c–f additionally presents the distribution of the elements utilized in the preparation of the cathode material on the electrode surface, depicted through image maps. The data indicate a relatively uniform dispersion of the individual elements across the electrode surface.

In addition to utilizing scanning electron microscopy and EDX for structural analysis, Raman spectroscopy was also employed. The Raman spectra (refer to Fig. 3a) of the prepared cathode material (green spectrum) reveal distinctly defined peaks. The characteristic vibrational modes of sulfur (red spectrum) are observed at wavelengths of 150, 216, and 470 cm^{-1}, with additional peaks corresponding to S_8 present at 245 and 434 cm^{-1} at very low intensities. The polypyrrole peaks are identified between the 1100 and 1600 cm^{-1} range. Specifically, the C = C bond stretching in ppy is indicated by a peak at 1576 cm^{-1}, the N-H bond bending at 1240 cm^{-1}, and the ring stretching of ppy at 1330 cm^{-1}. Additionally, two broad peaks at 1326 cm^{-1} and 1576 cm^{-1} correspond to the D and G band vibrations, respectively[21]. The intensity ratio of the D/G bands (ID/IG) was calculated to be 1.07 for carbon super P and 0.98 for the S/SP/ppy composite. The signal intensities were adjusted to enhance the readability of the spectra.

A complementary method to Raman spectroscopy is infrared spectroscopy. The infrared spectra of individual compounds used for the synthesis of polypyrrole and electrode material preparation are shown in Fig. 4a, and the assignment of characteristic absorption bands to vibrational modes is discussed further. The IR spectrum of pyrrole (see orange curve in Fig. 4a contains a broad absorption band located at 3391 cm^{-1} corresponding to υ(NH) vibration of the secondary amine, which was apparent by δ(NH) deformation vibration at 1677 cm^{-1}. Three absorption peaks at 3127, 3102 and 3052 cm^{-1} belong to the υ(CH) vibration of the heteroaromatic scaffold of pyrrole, which was also exhibited by three stretching υ(C = C/C-N) vibrations at 1529, 1468 and 1417 cm^{-1}, respectively. Polypyrrole (see blue curve in Fig. 4a showed vibrations similar to those of pyrrole and thus NH vibrations: stretching (3395 cm^{-1}) and deformation (1680 cm^{-1}), aromatic stretching υ(CH) at 3129, 3098 and 3048 cm^{-1} and three stretching υ(C = C/C-N) vibrations at 1531, 1471 and 1415 cm^{-1}. The υ(S–S) vibration in the region 470–480 cm^{-1} is the most prominent feature in the IR spectrum of elemental sulfur, corresponding to the stretching vibrations of the sulfur-sulfur bonds in the S_8 ring (see red curve in Fig. 4a and at 465 cm^{-1} corresponding to δ(SSSS)[22,23]. Super P carbon is a type of high surface area conductive carbon black used in batteries and other applications. In the IR spectrum (see black curve in Fig. 4a of Super P carbon the absorption bands in the region around 3000–3100 cm^{-1} could be attributed to aromatic hydrogen atoms ($υ(C–H)_{ar}$) and in

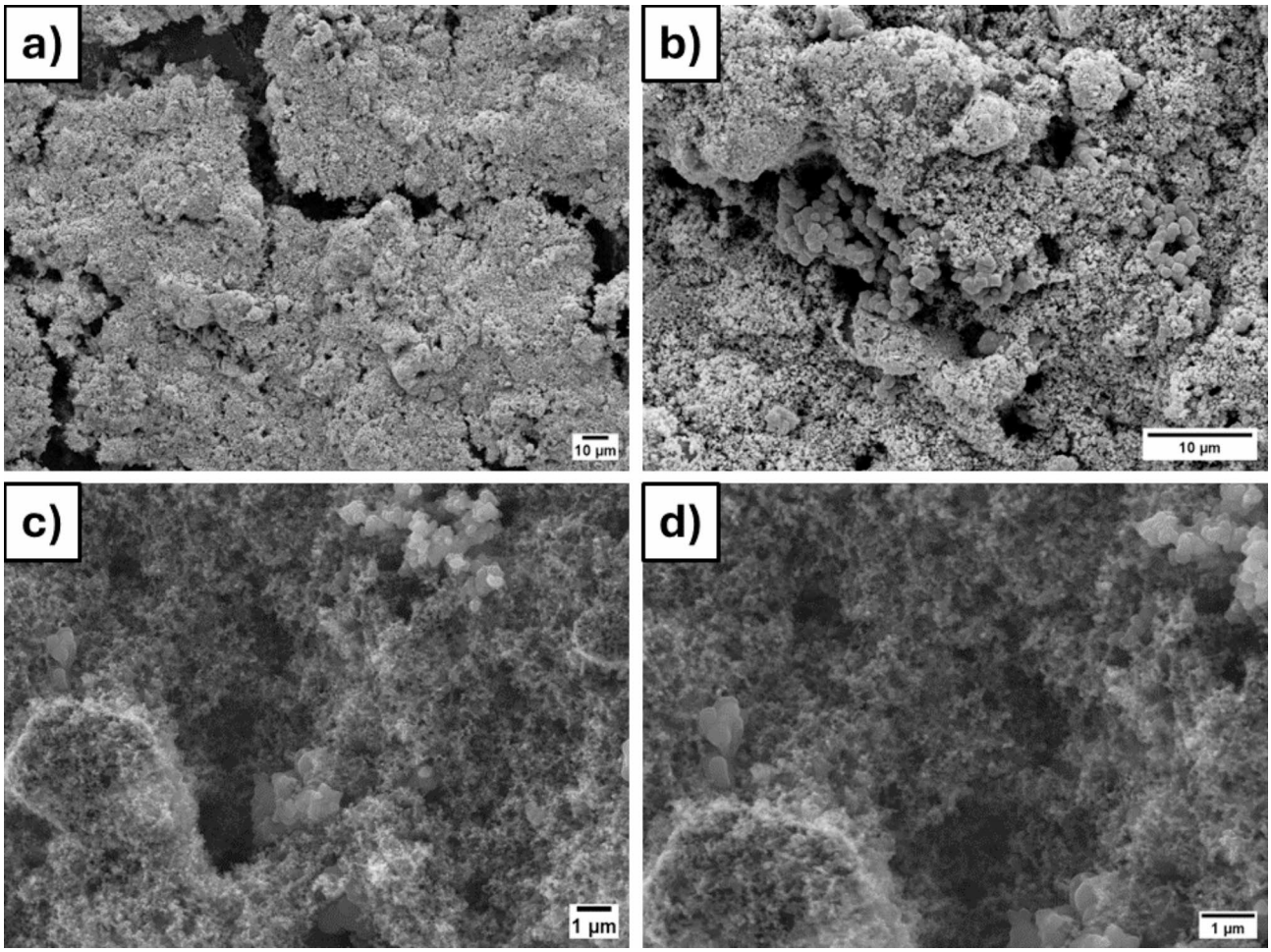

Fig. 1. SEM images of S/SP/ppy/PVDF electrode at magnifications of (**a**) 500x, (**b**) 2000x, (**c**) 5000x and (**d**) 10 000x, respectively.

the range 2800–3000 cm^{-1} to aliphatic C–H groups ($\upsilon(C–H)_{aliph}$). The absorption band around 1650–1750 cm^{-1} could indicate carbonyl groups (C=O), which are often present on the surface of oxidized carbon materials. The aromatic C=C stretching vibrations ($\upsilon(C=C)_{ar}$) located in the range of 1450–1600 cm^{-1}, indicating the presence of aromatic rings, which are common in carbon black structures. The IR spectrum of the S/SP/ppy electrode material (see green curve in Fig. 4a) contains mainly absorption bands of Super P carbon and sulfur, since their percentages are 60 and 25 wt%, respectively, and were higher than that of polypyrrole (15 wt%).

Thermal analysis was carried out to study the thermal stability of the individual components used to prepare the electrode material, as well as their percentage content after slurry preparation. The normalized TG curves of sulfur, polypyrrole, Super P and S/SP/ppy were measured in the temperature range of 150–800 °C and are shown in Fig. 4b. Since all the components are organic or inorganic in nature without presence of metals, no residual mass was observed after their thermal decomposition. In the case of pure sulphur, melting occurs at 113 °C followed by evaporation, resulting in a uniform one-step mass loss in the temperature interval 150–320 °C. Polypyrrole decomposed over a wider temperature range of 150–610 °C. The highest thermal stability was found for Super P carbon, which is thermally stable up to 640 °C and complete decomposition occurs at 785 °C in one step. Since the individual components show different thermal stability, it was possible to calculate their percentage in the prepared electrode material. Three distinct mass losses can be observed on the thermogravimetric curve of S/SP/Super P. Three distinct mass decays can be observed on the S/SP/Super P TG curve. The first mass loss of 60.9 wt% in the temperature interval 150–285 °C is attributed to sulphur, the second mass change of 15.2 wt% in the range 285–600 °C can be attributed to popypyrrole and the last mass decrease of 23.9 wt% in the interval 600–700 °C corresponds to Super P. The measured composition of the electrode material is in good agreement with the mass ratios used in the electrode material preparation: sulphur, carbon super P and polypyrrole (wt% 60:25:15). It should be noted that the thermal stability of the components in the electrode material is lower than that of the materials themselves and can be explained by partial amorphisation during the preparation process[24].

To conduct a more detailed investigation of the crystallographic structure, chemical composition, and physical properties of the prepared material, X-ray diffraction analysis was employed. Figure 3b presents the XRD patterns for the elemental sulfur powder, the prepared powdered polypyrrole, and the S/SP/ppy composite cathode material. The diffraction peaks of the as-prepared S/SP/ppy composite correspond closely

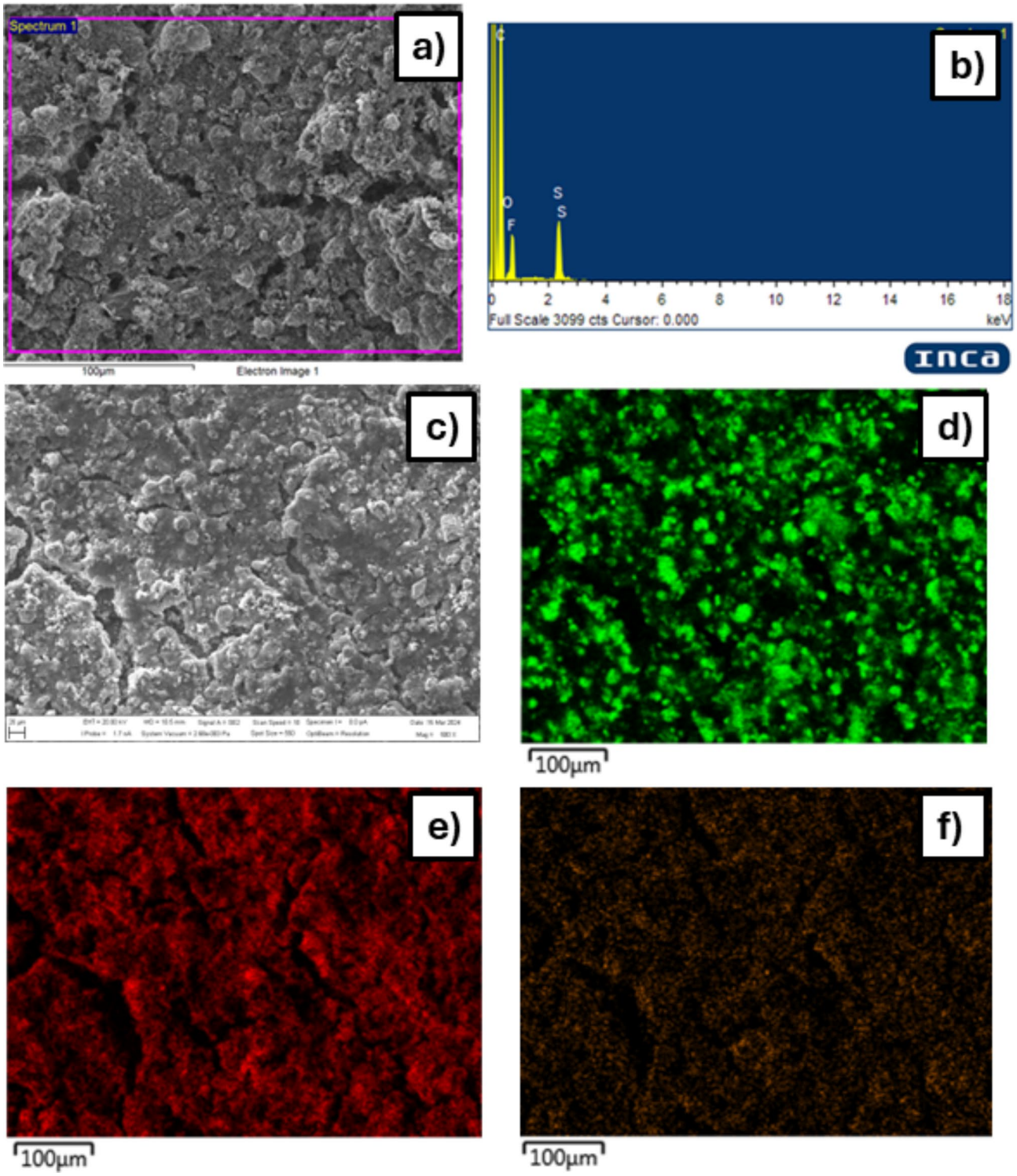

Fig. 2. EDX analysis and element mapping of the electrode: (**a**) analyzed area; (**b**) EDX spectrum; (**c**) analyzed area; (**d**) distribution of sulfur; (**e**) distribution of carbon and (**f**) fluorine.

with the standard diffraction peaks of sulfur, which can be attributed to the orthorhombic phase of sulfur. This observation indicates that no phase transformation of sulfur occurs during the incorporation of polypyrrole into the composite material.

Electrochemical analyses

Following the structural investigations, the electrochemical characteristics of the prepared positive electrodes were investigated. The test cells (El-Cell®) were built in the glove box filled with argon and an oxygen and water

	Weight %	Atomic %
C	73.52	83.95
O	1.85	1.59
F	13.34	9.63
S	11.28	4.83

Table 1. Summary of atomic and mass percentages of the individual elements.

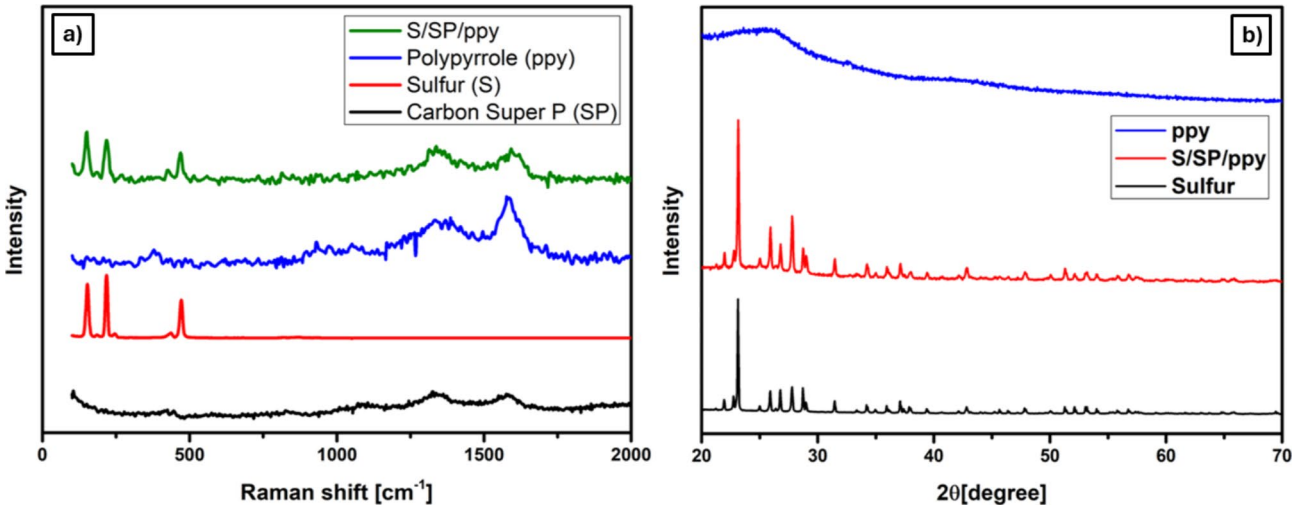

Fig. 3. (**a**) Raman spectra of S/SP/ppy composite material (green curve), sulfur (red curve), polypyrrole (blue curve) and carbon super P (black curve); (**b**) XRD spectra of S/SP/ppy composite material (red curve), sulfur (black curve) and polypyrrole (blue curve).

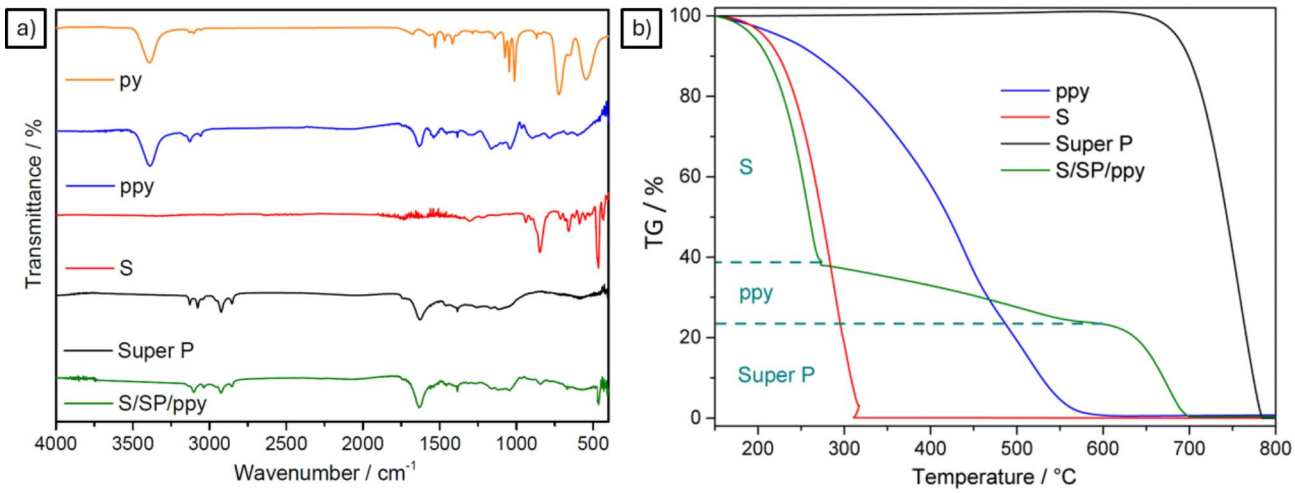

Fig. 4. IR spectra (**a**) of individual compounds used for the synthesis of polypyrrole and electrode material preparation (**b**) Thermogravimetric curve measured in an air atmosphere in the temperature range of 30–800 °C.

content below 10 ppm. Firstly, CV was used for examination of oxidation and reduction processes inside of battery cells within a potential range of 1.8 V to 2.8 V, with scan rates of 0.1; 0.5; 1 and 2 mV s^{-1}. The cyclic voltammogram recorded at 0.1 mV s^{-1} illustrated in the Fig. 5a (black curve) reveals two oxidation peaks at potentials of 2.3 V and 2.5 V, and two reduction peaks at potentials of 2.3 V and 1.9 V. These peaks correspond to the typical mechanism observed in Li-S batteries, where sulfur undergoes reduction to form polysulfides, which are subsequently oxidized back to S_8. The electrode demonstrates optimal system stability, as evidenced by the cyclic voltammogram recorded at 0.1 mV s^{-1} (Fig. 5a), where the cathodic and anodic peaks exhibit minimal

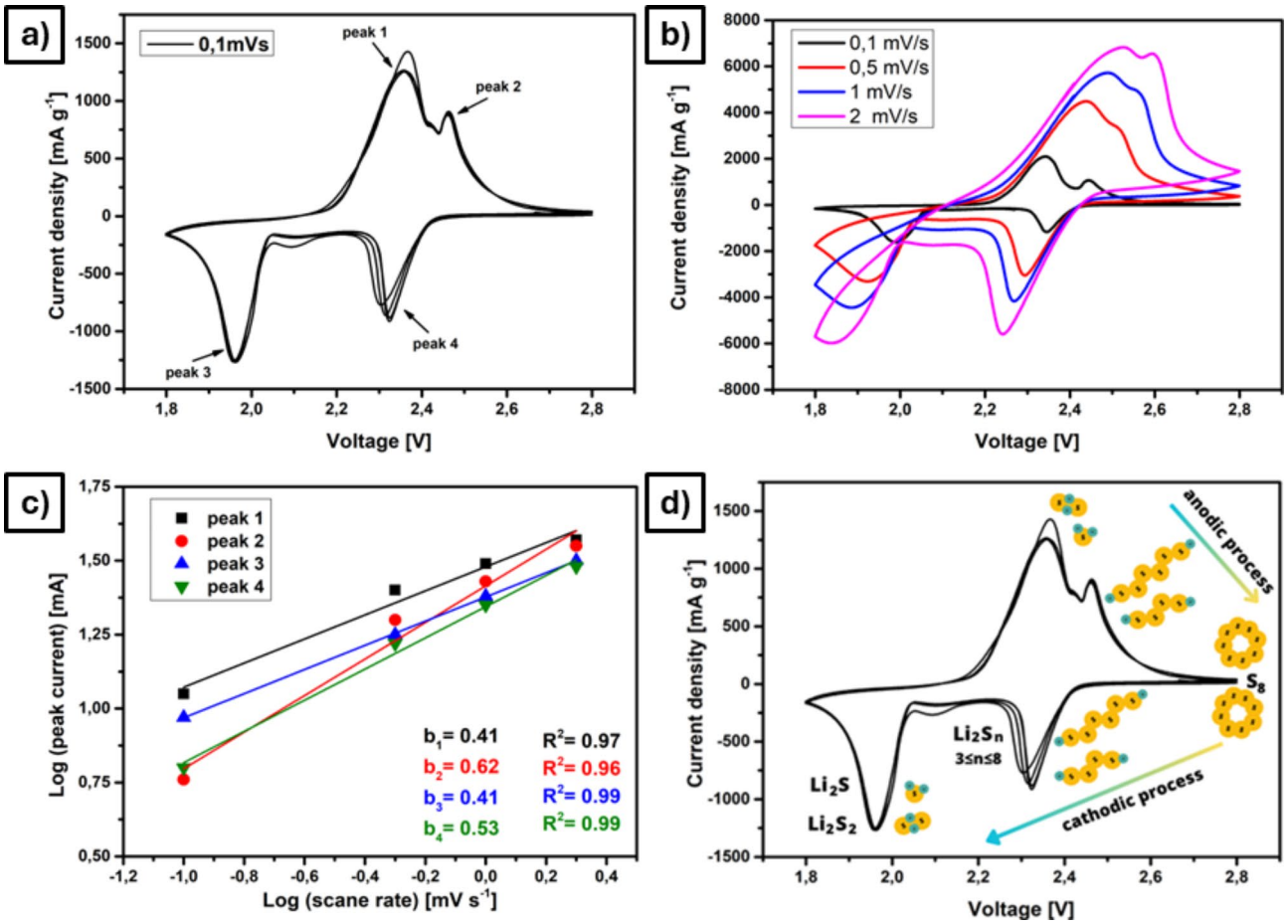

Fig. 5. CV curves of S/SP/ppy/PVDF electrode at (**a**) scane rate 0.1 mV s^{-1}; (**b**) at different scane rates (0.1, 0.5, 1 and 2 mV s^{-1}); (**c**) log of current response of individual peaks and the log of scan rates and (**d**) mechanism of anodic and cathodic processes inside the cell.

shift and almost overlap even after second cycle. Cyclic voltammograms at different scane rates were also recorded to assessment the S/SP/ppy/PVDF electrode kinetics of reactions (Fig. 5b). The peak intensity exhibits an upward trend with the increment of the scan rate, while the overall morphology of the cyclic voltammetry curve remains consistent. This result can also be attributed to good electrochemical stability. The Fig. 5c illustrates the relationship between the log of current response of individual peaks and the log of scan rates. The slopes of the resulting curves, which are 0.41, 0.62, 0.41, and 0.53 respectively, indicate a rapid diffusion of Li^+ ions[25]. Figure 5d represents the anodic and cathodic processes inside of the battery cell.

The charge/discharge process in case of sulfur cathode is not strictly related only to Li ion diffusion, but this process is characterized also by the formation of soluble polysulfides and solid Li_2S during discharge. The severe capacity-fades usually observed in Li–S batteries[26] were explained by the accumulation of irreversible Li_2S in the cathode with cycling and decreasing the available conductive ppy/carbon surface for the redox reaction with cycling. Moreover, the observed decrease in capacity with increasing current density can be ascribed to the restricted availability of Li^+ ions within the confined spaces of the electrode material[27].

Figure 6a presents plots depicting the variation in capacity as a function of the number of cycles at different C-rates (0.2 C, 0.5 C, 1 C, and 2 C), followed by measurements at the same C-rates in reverse order (1 C, 0.5 C, and 0.2 C). As the C-rate increases, the capacity of the S/SP/ppy/PVDF electrode gradually decreases from an initial capacity of 813 mAh g^{-1} at 0.2 C to 331 mAh g^{-1} at 2 C after 35 cycles. Detailed results are summarized in the accompanying Table 2, which shows that after 50 cycles, the capacity decreased by 5.45% relative to the first cycle. The graph in Fig. 6a clearly illustrates that there is no significant change in capacitance during cycling at various current densities, except for slight increases at 0.5 C and 1 C. These increases may be attributed to the sulfur stored in the matrix not being fully reacted. Specifically, at 1 C, there was an increase in capacity from 484 mAh g^{-1} (cycle 26) to 504 mAh g^{-1} (cycle 30), representing a 38% decrease in total capacity compared to the first cycle at 0.2 C. At 0.5 C, there was initially a slight increase in capacity followed by a decrease, amounting to a 20% decrease compared to the first cycle at 0.2 C. Overall, these results indicate that the polypyrrole-added electrode-maintained stability throughout the testing under varying loads.

Figure 6b illustrates the charge and discharge profiles resulting from galvanostatic cycling at various electrode loadings (C-rate: 0.2 C, 0.5 C, 1 C, and 2 C). Each discharge curve exhibits two characteristic plateaus, the first

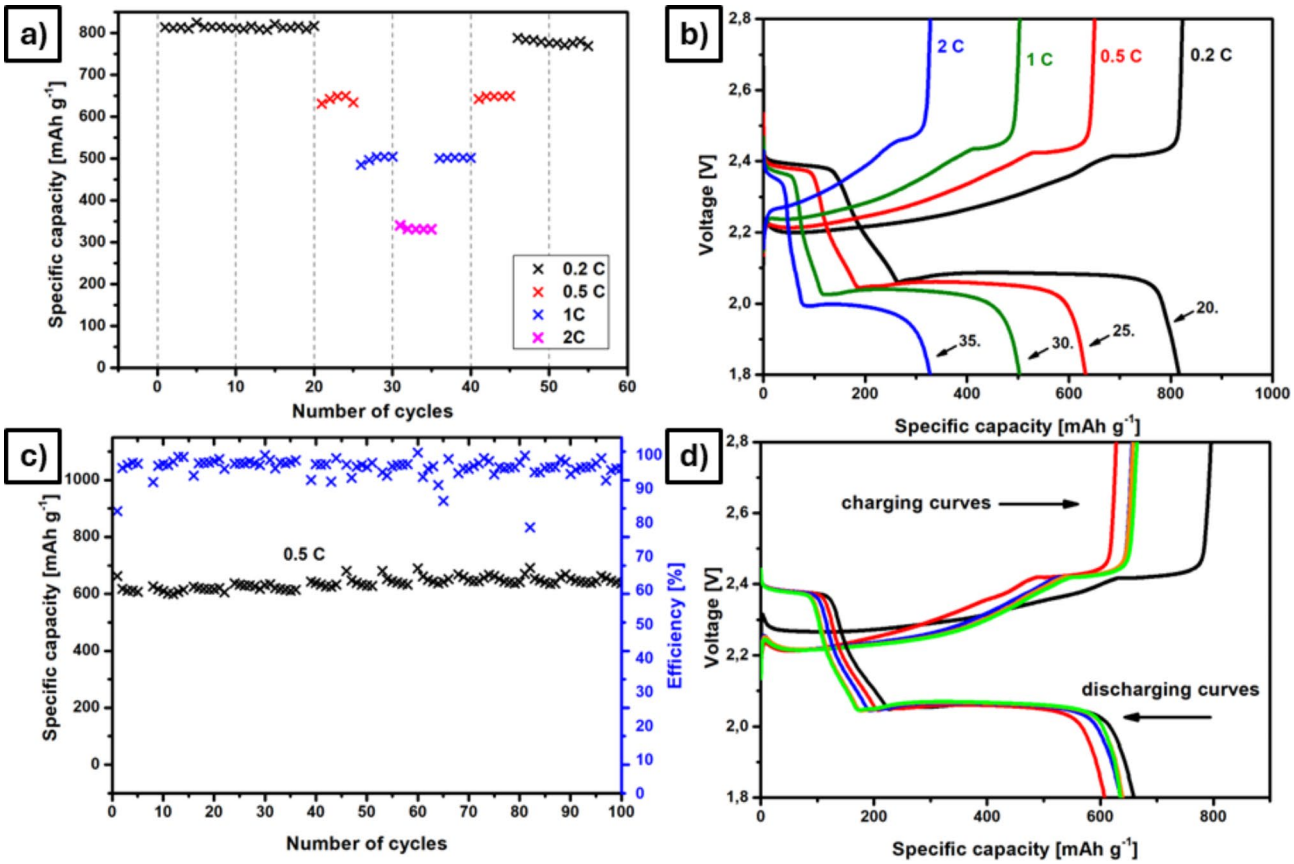

Fig. 6. (**a**) Capacity changes for S/SP/ppy/PVDF at different C-rates; (**b**) charge/discharge curves of S/SP/ppy/PVDF at different C-rates for the 20th cycle (black), 25th cycle (red), 30th cycle (green), and 35th cycle (blue); (**c**) long-term cycling results for S/SP/ppy/PVDF at 0.5 C (100 cycles) and corresponding (**d**) charge/discharge curves of long-term cycling.

C-rate	No. cycle	Specific capacity [mAh g^{-1}]	Capacity decrease vs. 1st cycle [%]
0.2 C	1	813.3	
0.2 C	20	816.9	+0.44
0.5 C	25	633.7	−22.08
1 C	30	504.6	−37.96
2 C	35	331	−59.3
1 C	40	501.3	−38.36
0.5 C	45	648.7	−20.24
0.2 C	50	775.6	−4.64
0.2 C	55	769	−5.45

Table 2. Capacity changes during galvanostatic cycling of S/SP/ppy/PVDF at various C-rates.

at 2.4 V and the second at 2 V, corresponding with the CV results and indicating different stages of polysulfide formation. The capacity of the cathode material decreases with increasing C-rate.

Long-term measurement results for the S/SP/ppy/PVDF cathode at a 0.5 C rate over 100 cycles are presented in Fig. 6c, along with the corresponding capacitances and efficiencies. The initial discharge capacity was 662 mAh g^{-1}, which decreased to 637 mAh g^{-1} after 100 cycles, maintaining an overall efficiency of 96% throughout the cycling period at 0.5 C. Figure 6c further demonstrates that the S/SP/ppy/PVDF electrode maintained a nearly constant capacity of 600 mAh g^{-1} during the cycling, with only occasional fluctuations, likely due to an undesired shuttle effect. This represents a mere 3.8% decrease in capacity compared to the initial 662 mAh g^{-1} after 100 cycles. These findings indicate the composite's cycling stability. Figure 6c display a slight fluctuation that could be explained by the catalytic properties of polysulfides as it was presented in previous studies where polysulfides catalyzes the redox reaction involving sulfur and lithium sulfide[28]. We suppose that the observed

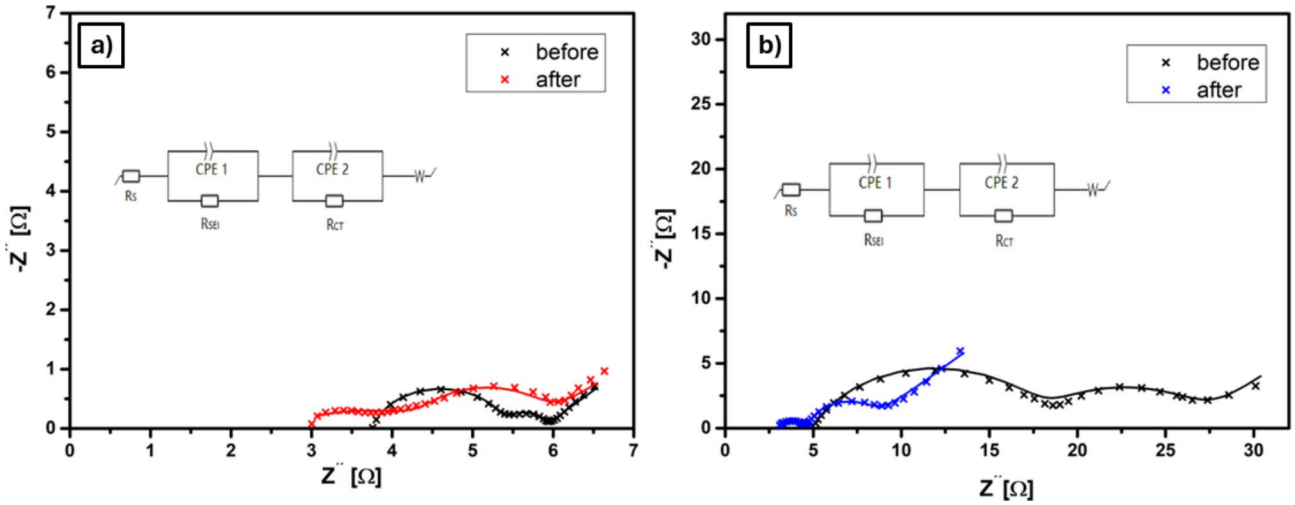

Fig. 7. (**a**) Nyquist plot of the El-cell electrode testing before and after 100 cycles with corresponding circuit and (**b**) Nyquist plot of the coin cell electrode testing before and after 100 cycles with corresponding circuit.

El-cell	R_S [Ω]	R_{ct} [Ω]	R_{SEI} [Ω]	CPE_1 [F]	CPE_2 [F]	χ^2 [Ω²]
Before	3.76	0.44	1.66	46.41 e^{-6}	3.53 e^{-3}	0.036
After	2.59	2.07	1.22	11.15 e^{-3}	10.33 e^{-3}	0.093
Coin cell						
Before	5.02	8.63	13.07	12.34 e^{-6}	1.72 e^{-3}	0.9
After	2.96	3.08	1.69	13.2 e^{-5}	1.49 e^{-3}	0.71

Table 3. Summary of results from the EIS measurements of El-cell and coin cell.

capacity fluctuations arise from the polysulfides trapping within the ppy cathode matrix. Upon reaching a critical concentration, the entrapped polysulfides is promoted to undergo redox reactions, contributing to an increase in capacity. Subsequently, a gradual decrease in capacity is observed as the trapped polysulfides undergoes dissolution. This cyclical process is believed to be responsible for the fluctuating capacity behavior.

As depicted in Fig. 6d, the S/SP/ppy/PVDF electrode demonstrates an initial discharge capacity of 662 mAh g^{-1}, which decreases to 637 mAh g^{-1} after 100 cycles at a C-rate of 0.5 C. The discharge curves consistently exhibit two distinct plateaus throughout the cycling process, substantiating the presence of elemental sulfur and polysulfides within the pores of the polypyrrole matrix, even after 100 cycles.

EIS spectra recorded for El-Cell and coin cell before and after cycling are shown in Fig. 7a. Equivalent circuit used to fit recorded data is shown in Fig. 7. and consists of solution resistance R_S, charge transfer resistance R_{ct}, and resistance of SEI layer R_{SEI} along with two constant phase elements CPE1 and CPE2 and Warburg element. Two depressed semicircles are attributed to SEI layer resistance (high frequency) and electrode-electrolyte interface resistance (intermediate frequency). Warburg is correlated to ion diffusion in the electrode.

Results of the fitting El-Cell EIS spectra (Table 3) indicate good charge transfer at electrode-electrolyte interface with R_{ct} value of 0.44 Ω. The increase of the R_{ct} after cycling (2.07 Ω) can mean development of cracks in the cathode or it can be correlated to the agglomerate creation[29]. Prepared El-cell demonstrated low R_{SEI} (1.66 Ω) before cycling and even lower value (1.22 Ω) after 100 cycles, suggesting creation of uniform SEI layer, which may be related (at least partial) elimination of shuttle effect.

The coin cell EIS spectra (Fig. 7b) show rapid decrease of resistance after 100 cycles compared to before cycling- R_{ct} dropped from 8.63 Ω (before) to 3.08 Ω (after) and R_{SEI} decreased from 13.07 Ω (before) to 1.69 Ω (after). The considerable resistance reduction may be attributed to electrochemical activation and/or uniform SEI formation. The dissolution of sulfur in the electrolyte could have been a contributing factor as well along with better contact caused by redistribution of ppy[30,31].

Through a detailed analysis of the EIS spectra, we were ablion coefficient (D) and the exchange current density (j_0). The exchange current density is a pivotal parameter that characterizes the reversibility of the electrode reaction. The diffusion coefficient can be quantified using a range of electrochemical methodologies. In this study, we employed EIS to ascertain this coefficient[32,33].

$$D = \frac{1}{2}\left[\frac{RT}{z^2F^2CA\sigma}\right]^2 \quad (1)$$

El-Cell	R_{ct} [Ω]	σ [Ω $s^{1/2}$]	j_0 [mA cm^{-2}]	D [cm^2 s^{-1}]
Fresh	0.44	0.54	1.48	2.39×10^{-9}
After 100 cycles	2.07	0.9	2.44	8.63×10^{-10}
Coin cell				
Fresh	8.63	5.99	0.58	1.95×10^{-11}
After 100 cycles	3.08	7.27	1.64	1.32×10^{-11}

Table 4. Summary of results from Eqs. (1) and (2).

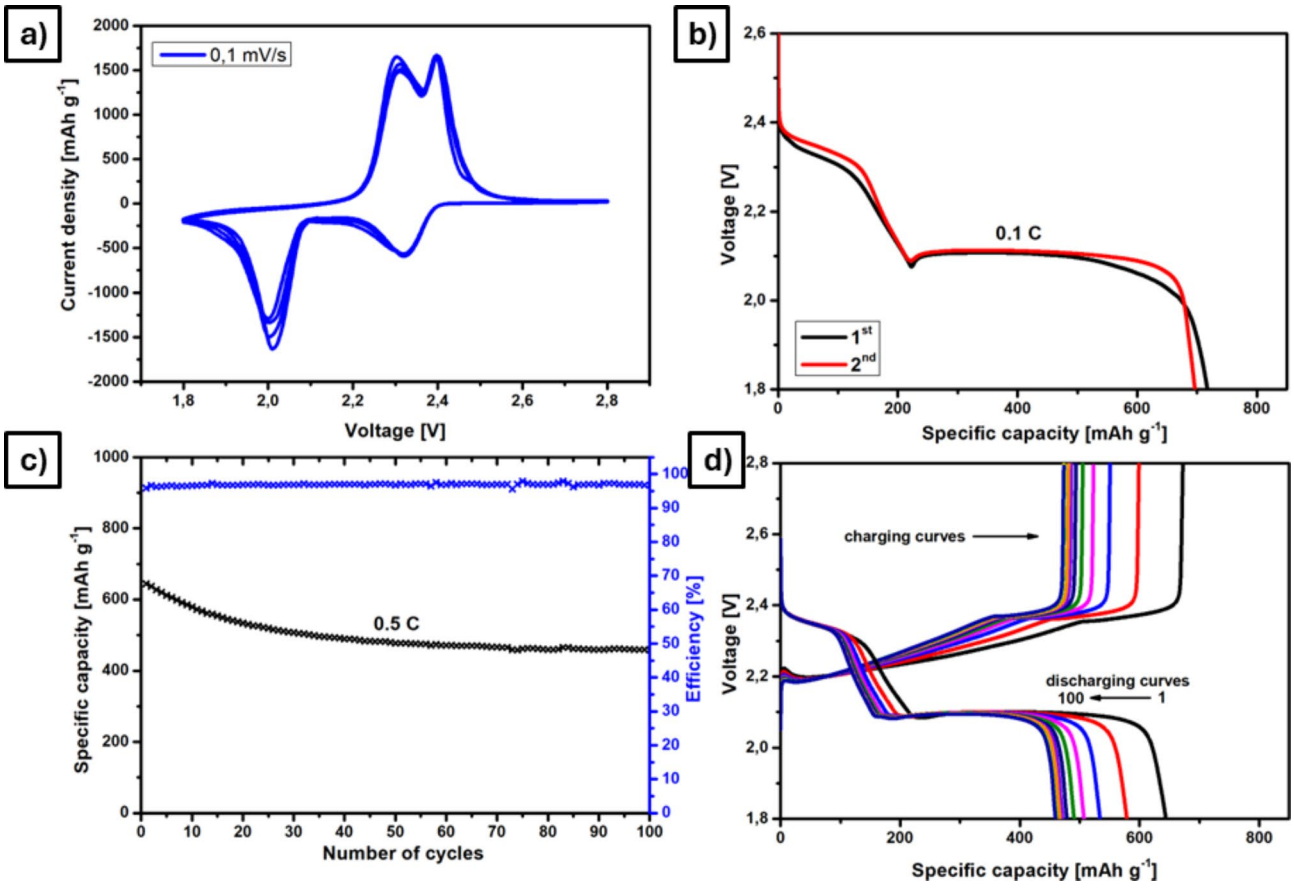

Fig. 8. (**a**) CV curves of S/SP/ppy/PVDF electrode at scane rate 0.1 mV s^{-1}; (**b**) initial discharge curves at 0.1 C (**c**) results from long-term cycling in coin cell for S/SP/ppy/PVDF electrode at 0.5 C (100 cycles) and (**d**) corresponding charge/discharge curves from long-term cycling.

$$j_0 = \frac{i_0}{A} = \frac{RT}{zFR_{ct}A} \tag{2}$$

Herein, R is the molar gas constant; T is the absolute temperature (20 °C in this work); z is number of electrons transferred during reaction; F is Faraday constant; C is concentration and A is surface area. Kinetics parameters of the S/SP/ppy/PVDF electrode are summarized in Table 4. By substituting Warburg coefficient (σ) into Eq. (1) and the charge transfer resistance (R_{ct}) to Eq. (2), the pre-cycling values of j_0 and D were found to be 9.36 mA cm^{-2} and 2.31×10^{-9} cm^2 s^{-1}, respectively. After 100 cycles, the post-cycling values for j_0 was 2.44 mA cm^{-2}, while for D it was 8.63×10^{-10} cm^2 s^{-1}.

Electrochemical coin cell measurements

As illustrated in the accompanying Fig. 8a, the cathodic process is characterized by the emergence of two primary peaks at approximately 2.3 V and 2.0 V. These peaks correspond to the transformation of elemental sulfur into longer-chain lithium polysulfides (Li_2S_n, where $n \geq 4$), followed by the conversion to shorter-chain polysulfides ($n < 4$), ultimately leading to the formation of Li_2S. During the anodic process, two distinct peaks are observed at potentials of 2.3 V and 2.4 V. The stability of the prepared material is evidenced by the consistent positions and intensities of these cathodic and anodic peaks across multiple cycles. The discharge curves, also

presented in the Fig. 8b, exhibit two plateaus at approximately 2.35 V and 2.1 V, which align with the features observed in the cyclic voltammogram. The S/SP/ppy/PVDF cathode demonstrates an initial discharge capacity at 0.1 C of approximately 717 mAh g^{-1}. In the subsequent phase of coin cell testing, we assessed the stability of the synthesized cathode incorporating polypyrrole over an extended cycling period at a constant C-rate (0.5 C; 100 cycles). The outcomes of this evaluation are illustrated in Fig. 8c. The S/SP/ppy/PVDF cathode demonstrated remarkable stability throughout the cycling process, maintaining an overall efficiency of 96% even after 100 cycles (Fig. 8d). This efficiency is comparable to that achieved during cycling in an El-Cell. Initially, the electrode exhibited a capacity of 644 mAh g^{-1}. After 100 cycles at a 0.5 C rate, the electrode retained a capacity of 459 mAh g^{-1}, corresponding to a capacity deterioration of 0.34% per cycle.

Conclusion

The aim of this work was to prepare and characterize polypyrolle composite cathode material for Li-S batteries. Easy and scalable room temperature polymerization method utilizing oxidizing agent $FeCl_3$ was used and prepared polypyrolle was employed as conductive polymer in sulfur-carbon cathode. Testing in laboratory El-Cell showed the initial discharge capacity at 0.1 C 817 mAh g^{-1}. During extended cycling at a rate of 0.5 C, the S/SP/ppy/PVDF cathode exhibited an initial specific capacity of 662 mAh g^{-1}. After 100 cycles, the specific capacity was retained at 637 mAh g^{-1}. The Coulombic efficiency over this period was maintained at 96%. Working coin cell prototype was assembled to demonstrate possibilities of industrial applications. Coin cell measurements corroborate great results obtained from long-term El-Cell testing. The initial capacity at 0.5 C was 644 mAh g^{-1}, which was comparable to the results obtained from El-Cell testing. However, after long-term cycling (100 cycles), the capacity measured in the coin cell decreased to 459 mAh g^{-1}. Despite this reduction in capacity, the coin cell maintained an efficiency of 96%, which is consistent with the efficiency observed in the El- Cell. Despite widespread use of conductive polymers and extensive studies on ppy additives in Li–S batteries, working prototypes are rarely explored. Herein, we prepared and tested coin cell prototype of Li–S battery with ppy. Addition of ppy successfully suppressed shuttle effect, which is a prominent issue in Li-S batteries. Ppy enhanced the performance of lithium-sulfur batteries due to its high affinity for lithium polysulfide (LiPS) adsorption what was confirmed by fluctuating capacity behavior. This study employed two distinct experimental configurations, namely El-cell and coin-cell, to evaluate the performance of polypyrrole-based systems. The results obtained from both setups were found to be comparable. Notably, the preparation of polypyrrole in this investigation was characterized by its simplicity and cost-effectiveness, contrasting with many existing research reports that often involve more complex procedures, such as elevated or reduced temperatures and the addition of various additives.

Data availability

Data are available upon request from corresponding author. Patent application "Carbonized and/or Activated Metal-Organic Framework Composite Electrodes for Lithium-Sulfur Batteries and Manufacturing Method thereof" was submitted in 2024.

Received: 9 July 2024; Accepted: 24 September 2024
Published online: 02 October 2024

References

1. Manthiram, A., Chung, S. H. & Zu, C. Lithium-sulfur batteries: Progress and prospects. *Adv. Mater.* **27** (12), 1980–2006. https://doi.org/10.1002/adma.201405115 (2015).
2. Chen, X. et al. Conducting polymers meet Lithium–sulfur batteries: Progress, challenges, and perspectives. *Energy Environ. Mater.* **6** (5), 1–24. https://doi.org/10.1002/eem2.12483 (2023).
3. Fu, Y., Su, Y. S. & Manthiram, A. Sulfur-polypyrrole composite cathodes for Lithium-sulfur batteries. *J. Electrochem. Soc.*https://doi.org/10.1149/2.027209jes (2012). 9, pp. A1420–A1424.
4. Wild, M. et al. Lithium sulfur batteries, a mechanistic review. *Energy Environ. Sci.* **8** (12), 3477–3494. https://doi.org/10.1039/c5ee01388g (2015).
5. Li, L. et al. Sulfur–Carbon Electrode with PEO-LiFSI-PVDF composite coating for high-rate and long-life Lithium–sulfur batteries. *Adv. Energy Mater.* **13** (36), 1–13. https://doi.org/10.1002/aenm.202302139 (2023).
6. Li, Z. et al. Lithiated metallic molybdenum disulfide nanosheets for high-performance lithium–sulfur batteries. *Nat. Energy.* **8** (1), 84–93. https://doi.org/10.1038/s41560-022-01175-7 (2023).
7. Ren, R. et al. Efficient sulfur host based on Sn doping to construct Fe2O3 nanospheres with high active interface structure for lithium-sulfur batteries, *Appl. Surf. Sci.* **613**, 156003 https://doi.org/10.1016/j.apsusc.2022.156003 (2022).
8. Niščáková, V. et al. Novel cu(II)-based metal–organic framework STAM-1 as a sulfur host for Li–S batteries. *Sci. Rep.* **14** (1), 1–16. https://doi.org/10.1038/s41598-024-59600-8 (2024).
9. Yi, Y. et al. A novel sulfurized polypyrrole composite for high-performance lithium-sulfur batteries based on solid-phase conversion. *Chem. Eng. J.* **466**, 143303. https://doi.org/10.1016/j.cej.2023.143303 (2023).
10. Raza, H. et al. Li-S batteries: challenges, achievements and opportunities. *Springer Nat. Singap.* https://doi.org/10.1007/s41918-023-00188-4 (2023).
11. Duan, J. et al. A flexible and free-standing Cl–-doped PPy/rGO film as cathode material for ultrahigh capacity and long-cycling sodium based dual-ion batteries. *Carbon N .Y.*. **184**, 836–845. https://doi.org/10.1016/j.carbon.2021.09.006 (2021).
12. Pang, A. L., Arsad, A. & Ahmadipour, M. Synthesis and factor affecting on the conductivity of polypyrrole: a short review. *Polym. Adv. Technol.* **32** (4), 1428–1454. https://doi.org/10.1002/pat.5201 (2021).
13. Chen, Y. & Wang, C. Designing High Performance Organic batteries. *Acc. Chem. Res.* **53** (11), 2636–2647. https://doi.org/10.1021/acs.accounts.0c00465 (2020).
14. Chavan, U. D., Prajith, P. & Kandasubramanian, B. Polypyrrole based cathode material for battery application. *Chem. Eng. J. Adv.* **12**, 100416. https://doi.org/10.1016/j.ceja.2022.100416 (2022).
15. Sun, T., Sun, Q. Q., Yu, Y. & Zhang, X. B. Polypyrrole as an ultrafast organic cathode for dual-ion batteries, *eScience*, **1**, 186–193. https://doi.org/10.1016/j.esci.2021.11.003 (2021).

16. Dutta Pathak, D., Mandal, B. P. & Tyagi, A. K. A new strategic approach to modify electrode and electrolyte for high performance Li–S battery. *J. Power Sources*. **488**, 229456. https://doi.org/10.1016/j.jpowsour.2021.229456 (2021).
17. Luna-Lama, F., Caballero, A. & Morales, J. Synergistic effect between PPy:PSS copolymers and biomass-derived activated carbons: a simple strategy for designing sustainable high- performance Li–S batteries. *Sustain. Energy Fuels*. **6**, 1568–1586. https://doi.org/10.1039/D1SE02052H (2022).
18. Li, F. et al. Uniform polypyrrole layer-coated Sulfur/Graphene aerogel via the Vapor-Phase Deposition Technique as the Cathode Material for Li-S batteries. *ACS Appl. Mater. Interfaces*. **12** (5), 5958–5967. https://doi.org/10.1021/acsami.9b20426 (2020).
19. Wei, W. et al. Hierarchically porous SnO2 nanoparticle-anchored polypyrrole nanotubes as a high-efficient Sulfur/Polysulfide trap for high-performance Lithium-sulfur batteries. *ACS Appl. Mater. Interfaces*. **12** (5), 6362–6370. https://doi.org/10.1021/acsami.9b18426 (2020).
20. Zauška, L. et al. Adsorption and Release properties of Drug Delivery System Naproxen-SBA-15: Effect of Surface Polarity, Sodium/Acid Drug Form and pH. *J. Funct. Biomater.* **13** (4). https://doi.org/10.3390/jfb13040275 (2022).
21. Liang, X. et al. Split-half-tubular polypyrrole@sulfur@polypyrrole composite with a novel three-layer-3D structure as cathode for lithium/sulfur batteries. *Nano Energy*. **11**, 587–599. https://doi.org/10.1016/j.nanoen.2014.10.009 (2015).
22. Capková, D. et al. Influence of metal-organic framework MOF-76(gd) activation/carbonization on the cycle performance stability in Li-S battery. *J. Energy Storage*. **51, no.**https://doi.org/10.1016/j.est.2022.104419 (2022).
23. Nakamoto, K. Infrared and Raman Spectra of Inorganic and Coordination Compounds: Part A: Theory and Applications in Inorganic Chemistry https://doi.org/10.1002/9780470405840 (2008).
24. Pevná, V. et al. Redistribution of hydrophobic hypericin from nanoporous particles of SBA-15 silica in vitro, in cells and in vivo. *Int. J. Pharm.* https://doi.org/10.1016/j.ijpharm.2023.123288 (2023).
25. Yang, J. et al. September., Preparation of polyaniline-coated cobalt nitride nanoflowers as sulfur host for advanced lithium–sulfur battery, *J. Alloys Compd.* **981**,173701 https://doi.org/10.1016/j.jallcom.2024.173701 (2023).
26. Noh, H., Song, J., Park, J. K. & Kim, H. T. A new insight on capacity fading of lithium-sulfur batteries: the effect of Li2S phase structure. *J. Power Sources*. **293**, 329–335. https://doi.org/10.1016/j.jpowsour.2015.05.072 (2015).
27. Geng, P. et al. Polypyrrole coated hollow metal-organic framework composites for lithium-sulfur batteries. *J. Mater. Chem. A*. **7**, 19465–19470. https://doi.org/10.1039/c9ta05812e (2019).
28. Wang, L., Wang, Y. & Xia, Y. A high performance lithium-ion sulfur battery based on a Li2S cathode using a dual-phase electrolyte. *Energy Environ. Sci.* **8** (5), 1551–1558. https://doi.org/10.1039/c5ee00058k (2015).
29. Deng, Z. et al. Electrochemical Impedance Spectroscopy Study of a Lithium/Sulfur battery: modeling and analysis of Capacity Fading. *J. Electrochem. Soc.* **160** (4), A553–A558. https://doi.org/10.1149/2.026304jes (2013).
30. Majumder, S., Shao, M., Deng, Y. & Chen, G. Two dimensional WS 2 /C nanosheets as a Polysulfides immobilizer for high performance Lithium–sulfur batteries. *J. Electrochem. Soc.* **166** (3), A5386–A5395. https://doi.org/10.1149/2.0501903jes (2019).
31. Wang, G. et al. Improved electrochemical behavior of Li–S battery with functional WS2@PB–PPy–modified separator. *Chem. Eng. J. Adv.* **8**, 100145. https://doi.org/10.1016/j.ceja.2021.100145 (2021).
32. Wang, L., Zhao, J., He, X. & Wan, C. Kinetic investigation of sulfurized polyacrylonitrile cathode material by electrochemical impedance spectroscopy. *Electrochim. Acta*. **56**, 5252–5256. https://doi.org/10.1016/j.electacta.2011.03.009 (2011).
33. Lama, F. L., Marangon, V., Caballero, Á., Morales, J. & Hassoun, J. Diffusional features of a Lithium-sulfur battery exploiting highly Microporous activated Carbon. *ChemSusChem*. **16** (6). https://doi.org/10.1002/cssc.202202095 (2023).

Acknowledgements

This work was supported by the projects APVV-20-0138 and APVV-20-0111, by the VEGA project No. 1/0095/21 and KEGA project 002UPJS-4/2024.

Author contributions

V.N.: Investigation, Sample synthesis, Data curation, Writing-original draft; A.G.: Investigation, Writing—original draft, reviewing and editing; O.P.: Data curation; H.F.: Coin cell assembly; M.A.: Investigation, Data curation, Validation, Writing— reviewing and editing A.S.F.: Writing—reviewing and editing, Supervision, and Funding acquisition. All authors reviewed the manuscript.

Declarations

Competing interests

The authors declare no competing interests.

Additional information

Correspondence and requests for materials should be addressed to A.S.F.

Reprints and permissions information is available at www.nature.com/reprints.

Publisher's note Springer Nature remains neutral with regard to jurisdictional claims in published maps and institutional affiliations.